CHEMISTRY
A European Journal

A Journal of ChemPubSoc Europe

Title: n-Channel Organic Semiconductors Derived from Air-Stable Four-Coordinate Boron Complexes of Substituted Thienylthiazoles

Authors: Reinhard Hecht, Juliane Kade, David Schmidt, and Agnieszka Nowak-Król

To be cited as: *Chem. Eur. J.* 10.1002/chem.201701922

Link to VoR: http://dx.doi.org/10.1002/chem.201701922

Supported by ACES

WILEY-VCH

Chemistry - A European Journal

10.1002/chem.201701922

WILEY-VCH

FULL PAPER

n-Channel Organic Semiconductors Derived from Air-Stable Four-Coordinate Boron Complexes of Substituted Thienylthiazoles

Reinhard Hecht,[a,b] Juliane Kade,[b] David Schmidt,[a,b] and Agnieszka Nowak-Król*[a,b]

Abstract: Three acceptor-π-bridge-acceptor (A-π-A) molecules derived from 2-(3-boryl-2-thienyl)thiazole have been synthesized and thoroughly characterized. Incorporation of a B-N unit into thienylthiazole and attachment of suitable acceptor moieties allowed to obtain ambient-stable A-π-A molecules with low-lying LUMO levels. Their potential for applications in organic electronics was tested in vacuum-deposited organic thin film transistors (OTFT). The OTFT device based on boryl-thienylthiazole and 1,1-dicyanomethylene-3-indandione (DCIND) acceptor moieties showed an electron mobility of ~1.4 × 10^{-2} cm^2 V^{-1} s^{-1} in air, which is the highest electron mobility reported to date for organoboron small molecules. Conversely, the device employing the malononitrile (MAL) derivative as an active layer did not show any charge transport behavior. As suggested by single crystal X-ray analysis of indandione (IND) and MAL derivatives, the enhanced mobility of IND (and DCIND) in comparison to the MAL molecule can be attributed to the effective two-dimensional π-stacking in the solid state imparted by the acceptor moieties with an extended π-surface.

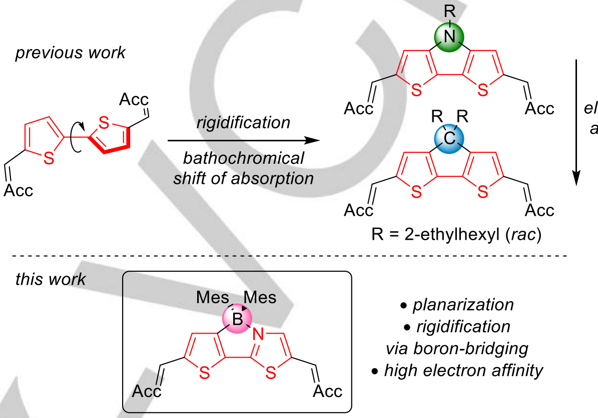

Figure 1. Design strategy towards electron-transport materials.

Introduction

A strong electron-accepting ability of boron endows organic aromatic scaffolds with valuable photophysical and electronic properties, such as low energies of the lowest unoccupied molecular orbitals (LUMOs), increased electron affinity, and both bathochromically shifted absorption and emission spectra.[1] These properties in combination with high fluorescence efficiency account for the rapid progress in the field of organoboron materials over the last twenty years. Accordingly, three- and four-coordinate boron complexes were intensively investigated for applications in organic light emitting diodes (OLEDs),[2] organic lasers,[3] nonlinear optics,[1a,4] fluorescence imaging[5] as well as photoresponsive materials,[6] and memory devices.[7] In addition, a strong electron affinity of three-coordinate boron with the vacant p-orbital on the boron center makes them attractive molecules for anion sensing.[8] On the other hand, due to a strong Lewis acidity, three-coordinate boron compounds are intrinsically sensitive to attack of nucleophiles, such as water, which limits the application of these organoboron materials.[1a,b,9] Common strategies that are applied to circumvent this problem aim either at protecting the boron center by bulky substituents[1b,10] or embedding a boron atom in a rigid π-conjugated scaffold.[11] Nevertheless, in terms of chemical and air-stability four-coordinate boron compounds are, in general, superior. In the boron-bridged molecules, this stabilization is imparted by the donation of a lone pair of an appropriately located heteroatom to the empty boron orbital, hence forming an electronically saturated compound. Importantly, boron-bridging increases rigidity of the molecular framework and extends the π-conjugated system, often by keeping two subunits of the molecule in a planar arrangement. A strong conformational constraint caused by chelation to the boron atom is an essential tool for tailoring photophysical properties of the parent systems.

To date, a plethora of four-coordinate boron compounds bearing different ligands and substituents on the boron atoms have been synthesized. In this group of compounds a choice of the ligand and boron substituents is, however, also critical for stability and properties. For instance, some BF_2 complexes of diketonates undergo hydrolysis in contact with moisture,[12] while sterically demanding mesityl (Mes) substituents on the boron center can induce stimulus-responsive material behavior.[13] Yet, there are plenty of molecules whose exciting photophysical features can be explored in air- and moisture-stable devices, mainly in OLEDs, or as imaging materials. More specifically, some BODIPY derivatives have been commercialized and are sold as fluorescent biological labels (Invitrogen BODIPY® dyes[14] or CHROMIS 500 N dyes).[15]

In our studies on electron-transport and acceptor materials for organic electronics we were looking for interesting platforms that would display favorable properties, such as low-lying LUMO

---

[a] R. Hecht, Dr. D. Schmidt, Dr. A. Nowak-Król
Center for Nanosystems Chemistry (CNC) & Bavarian Polymer Institute (BPI)
Universität Würzburg
Theodor-Boveri-Weg, D-97074 Würzburg (Germany)
E-mail: agnieszka.nowak-krol@uni-wuerzburg.de
[b] R. Hecht, J. Kade, Dr. D. Schmidt, Dr. A. Nowak-Król
Institut für Organische Chemie
Universität Würzburg
Am Hubland, D-97074 Würzburg (Germany)

Supporting information for this article can be found under http://dx.doi.org/10.1002/chem.2017xxxxx.

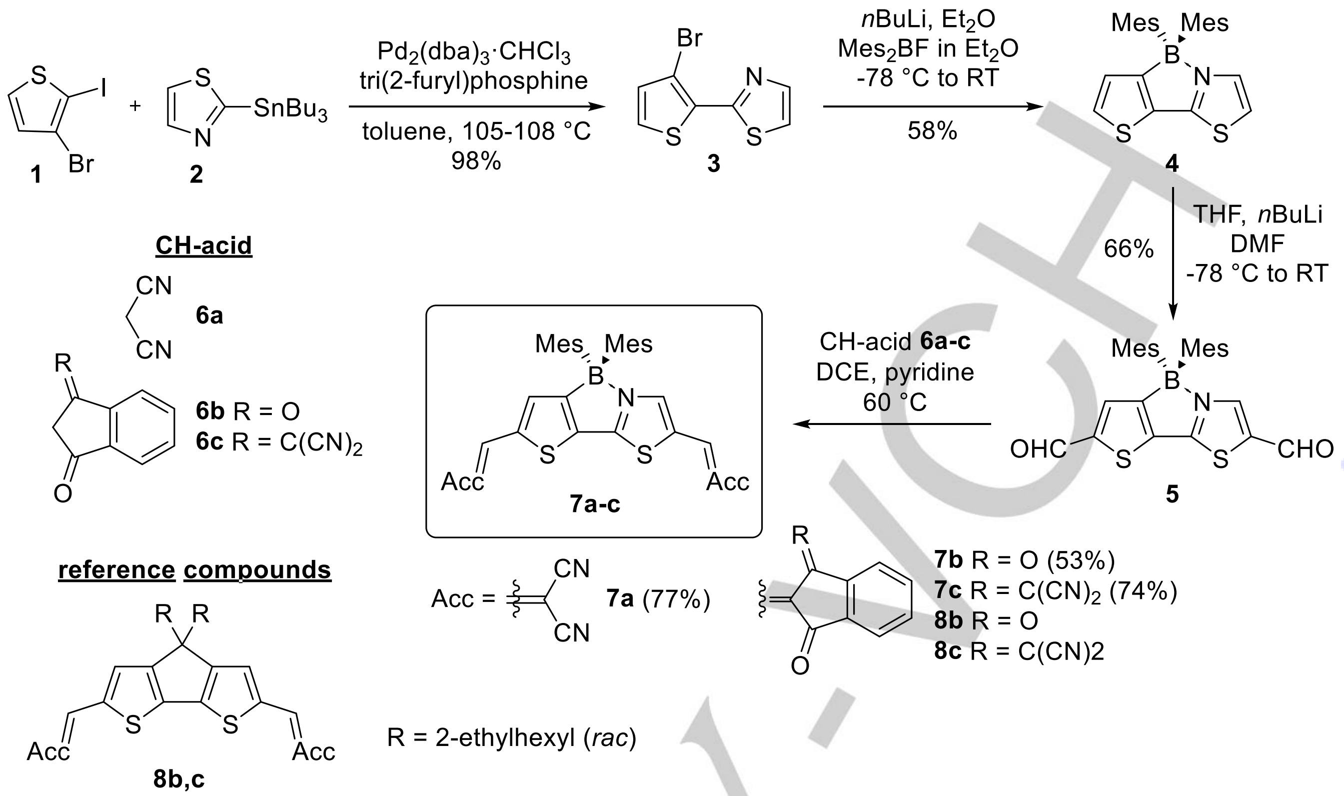

Scheme 1. Synthesis of A-π-A dyes with B-N dative bonds.

levels and high tunability of optical and electrochemical properties, which upon chemical functionalization would provide materials of suitably adjusted frontier molecular orbital (FMO) levels. Previously, we investigated dithienopyrrole and cyclopentadithienyl (CPDT) derivatives and observed a decrease of HOMO/LUMO levels by ca. 0.3 eV upon replacement of nitrogen for carbon as a bridging atom (Figure 1).[16] In this work, we planned to utilize boron to tune photophysical and charge transport properties of the π-core. Four-coordinate boron molecules in view of their valuable features appear to be well-suited molecules for our studies. Accordingly, we selected (3-boryl-2-thienyl)-2-thiazole for the central unit of A-π-A systems (see Figure 1). This scaffold, first introduced by Yamaguchi and co-workers, combines a common tendency of boron complexes to lower the LUMO level with the intrinsically high electron affinity of *N*-heterocyclic aromatic compounds containing C-N double bonds. Its potential as a building block for n-type organic semiconductors was verified by showing moderate electron mobility ($\mu_n = 1.5 \times 10^{-4}$ cm^2 V^{-1} s^{-1}) for one of three dimeric boryl-thienylthiazoles.[17] Later, Liu and co-workers inserted this interesting core into long polymer chains with alternating boron-bridged thienylthiazole and acceptor units.[18] Some of the new boron-containing polymers were utilized as acceptors in organic solar cells. Despite these prominent demonstrations, polymeric materials have some deficiencies when compared to small molecules. That is, the individuality of the repeating unit is lost in the polymer. Moreover, polydispersity along with a formation of various regioisomers (i.e. head-to-tail, and head-to-head bonding modes) limit the possibility to gain deeper insight into the basic optical and electrochemical properties of a particular repeating unit, whereas small molecules benefit from well-defined molecular structures, high reproducibility and purity without batch to batch variations.

The properties of this platform in small molecules have been elucidated only for dimeric regioisomers described by Yamaguchi,[17] and very recently, for π-conjugated systems reported by Wakamiya.[19] Herein, we describe the synthesis, optical, electrochemical and structural characterization of a set of A-π-A molecules derived from 2-(3-boryl-2-thienyl)thiazole. In this work we were particularly interested whether the introduction of this boron-heterocyclic core into A-π-A systems would provide the opportunity for fine-tuning FMOs to the level required for ambient stable n-channel semiconductors or acceptor materials for photovoltaics. As we will show, by a proper combination of the acceptor unit and boryl-substituted thienylthiazole, we were able to obtain an electron-transport material which was successfully utilized in organic field effect transistors (OFET), showing the highest electron mobility observed to date for OFET devices based on organoboron small molecules.

Results and Discussion

Design considerations and synthesis. Our molecular design of A-π-A molecules assumes attachment of two identical acceptor units to a thienylthiazyl-boron-core serving here as a π-bridge. To this end, we have selected three acceptor moieties, i.e. malononitrile, commonly used in organic electronics, and two CH-acids: indandione (IND) and 1,1-dicyanomethylene-3-indandione (DCIND) with a rigid framework and extended aromatic surface. Previously, we utilized the latter methylene compounds in A-π-A systems based on dithienopyrrole and cyclopentadithienyl

10.1002/chem.201701922

cores.[16] They also proved effective to tune FMO levels and a packing arrangement in a large variety of merocyanines.[20] An introduction of electron-withdrawing substituents was performed by Knoevenagel condensation between dialdehyde boryl-substituted thienylthiazole and respective methylene compounds. Thus, in contrast to previous 2-(3-boryl-2-thienyl)thiazole derivatives,[17-18] the boryl-substituted π-scaffold and acceptor components are intervened by ethylene linker to ensure full coplanarity and enhance the conjugation. Lastly, we decided to introduce mesityl groups on the boron center, which endowed the synthesized compounds with excellent stability and good solubility required to pursue these studies.

The synthetic route towards A-π-A molecules with boron-nitrogen dative bond is illustrated in Scheme 1. 3-Bromo-2-iodothiophene (**1**)[21] and 2-(tributylstannyl)thiazole (**2**)[22] were prepared according to the reported procedures. Stille reaction of these coupling partners in toluene afforded thienylthiazole **3** in the excellent yield of 98%. Subsequent lithiation thereof, followed by the reaction with Mes_2BF was performed in a similar fashion to the procedure reported by Yamaguchi and co-workers.[17] Functionalization of dimesitylboryl compound **4** with *n*BuLi and DMF produced dialdehyde **5** in 66% yield. Finally, Knoevenagel condensation between CH-acids **6a-c** and dialdehyde **5** afforded three target molecules **7a-c** in moderate to good yields. To ensure high conversion rate we used 2 eq. of the methylene compounds per formyl group.

Solid state structural analysis. Single crystals of **7b** suitable for X-ray analysis were obtained by slow evaporation of toluene (Figure 2c,d) at room temperature. The dihedral angle between thiophene and thiazole rings is 3.3°, which shows that the two fragments are nearly co-planar. The dihedral angles between indandione unit and a boryl core mean plane linked by vinylene bridge are 2.1° and 2.0° on the side of thiophene and thiazole, respectively. Hence, the acceptor moieties are effectively conjugated to the boryl central core. The crystal of **7a** was obtained by slow evaporation of CD_2Cl_2 at room temperature. The dihedral angle between thiophene and thiazole ring is 4.4°, which is comparable to that in **7b**. The acceptor units are twisted out of the mean plane of the thienylthiazole-boron core by 11.1° and 4.3° on the sides of thiophene and thiazole, respectively (Figure 2a,b). The B-N and B-C(thiophene) bond lengths are 1.650(2) and 1.645(2) Å, respectively, and both B-C(Mes) bond lengths are 1.637(2) and 1.638(2) Å in the crystal of **7b**. Equal lengths of B-N, B-C(thiophene) bonds were observed in the crystal of **7a** (1.647(5) Å), while the two B-C(Mes) bonds were 1.643(5) Å and 1.629(5) Å long. Boron atoms in both cases adopt a distorted tetrahedral geometry to form N,C-chelate five membered rings. Thienylthiazole ligands display smaller C(thiophene)-B-N angles than the ideal angle of 109.5°. The corresponding values are 94.2(1)°, and 93.7(3)°in molecules **7b**, and **7a**, respectively. Conversely, the C(Mes)-B-C(Mes) angles (115.4(1)° in **7b** and 120.2(3)° in **7a**) are larger than the ideal angle. The details of the X-ray measurements and the crystal data are described in the Supporting Information.

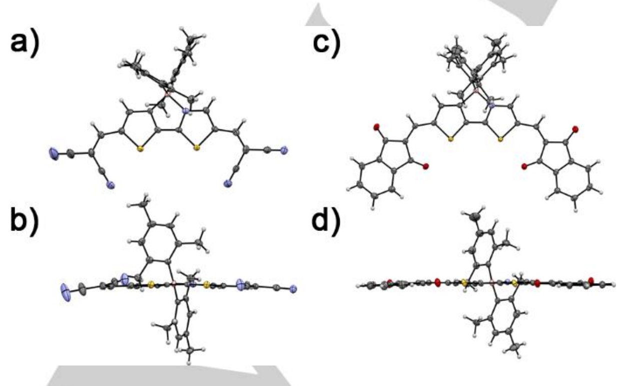

Figure 2. Solid-state molecular structures determined by single-crystal X-ray diffraction of compound **7a** obtained from CD_2Cl_2 a) front view, b) side view, and compound **7b** obtained from toluene c) front view, d) side view; ellipsoids set at 50% probability. Crystal of **7b** contains toluene molecules.

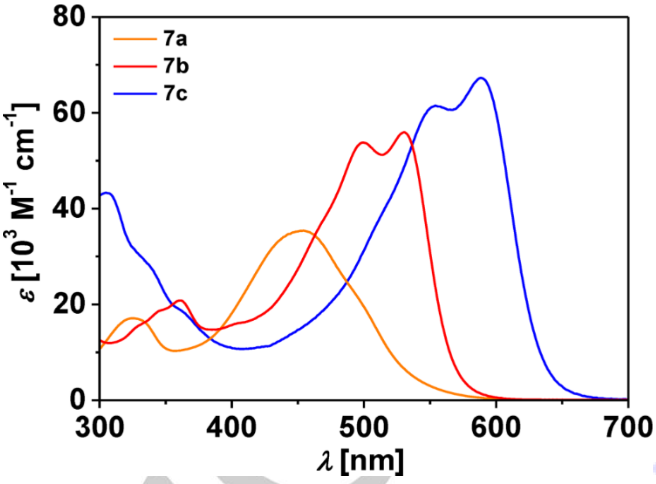

Figure 3. UV/Vis absorption spectra of dyes **7a-c** measured at $c \sim 10^{-5}$ M in CH_2Cl_2.

Absorption properties. Optical properties of A-π-A dyes **7a-** were investigated by steady-state absorption and emissio spectroscopy in methylene chloride. The UV/Vis absorption spectr are shown in Figure 3 and the data are listed in Table 1. All A-π- dyes feature moderate to high absorption coefficients in the rang of 3.5 x 10^4 to 6.7 x 10^4 M^{-1} cm^{-1}. The corresponding squar transition dipole moments μ^2_{eg} of dyes **7a**, **7b**, and **7c** are 82, 118 and 140 D^2, respectively. Compound **7a** exhibits an orange color i solution (Figure S1), which corresponds to a broad absorption ban located at 454 nm with a shoulder at ca. 495 nm. In comparison t

Table 1. Optical and electrochemical properties of dyes **7a-c** and **8b,c**.

Dye	λ_{abs}[a] [nm]	ε_{max}[b] [10^4 M^{-1} cm^{-1}]	μ^2_{eg}[c] [D^2]	$E^{red}_{1/2}$[d] [V]	$E^{ox}_{1/2}$[d] [V]
7a	454	3.5	82	–1.00, –1.25	+0.91[e]
7b	530	5.6	118	–1.12, –1.49[e]	+0.89,[e]
	499	5.4			+1.01,[e] +1.17[e
7c	589	6.7	140	–0.84[e,f]	+0.90[e]
	554	6.2			
8b[16]	584	12.2	138	–1.30	+0.84
8c[16]	664	13.1	167	–0.84[e]	+1.08

[a] Absorption maximum and vibronic progression in CH_2Cl_2. [b] Molar absorption coefficient in CH_2Cl_2. [c] Square transition dipole moment calculated for the lowest energy transition of the UV/Vis absorption spectrum in CH_2Cl_2. [d] Redox potentials were measured in dry CH_2Cl_2 ($c \sim 10^{-4} - 10^{-5}$ M) at a scan rate of 100 mV s^{-1} and with 50% of iR compensation; supporting electrolyte Bu_4NPF_6 (c = 0.1 M). Measurements were calibrated vs. the ferrocenium/ferrocene (Fc^+/Fc) redox couple as an internal standard. [e] Peak potential. [f] Further reduction processes were observed but peak potentials could not be resolved.

10.1002/chem.201701922

molecule **7a**, the lowest-energy absorption bands of **7b** and **7c** are bathochromically shifted. This is due to the extension of the conjugated system in **7b,c**. Furthermore, a larger shift observed for **7c** can be attributed to a stronger electron accepting nature of the DCIND vs. IND moieties. Solution of **7b** and **7c** exhibit red and purple colors in CH_2Cl_2 (Figure S1). The spectra of these compounds reveal broad absorption bands centered at 530 nm and 589 nm, respectively, with vibronic progressions at 499 for **7b**, and 554 nm for **7c**. The emission of **7a-c** was effectively quenched in CH_2Cl_2. These results may suggest charge transfer (CT) interactions as one of the possible deactivation pathways for all three A-π-A systems.

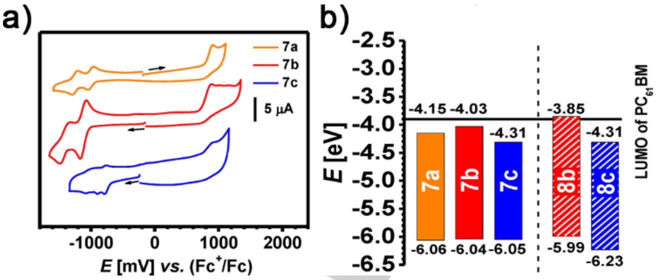

Figure 4. a) Cyclic voltammograms of **7a-c** calibrated versus ferrocenium/ferrocene (Fc^+/Fc) (c ~ 10^{-4} – 10^{-5} M in dry CH_2Cl_2; scan rate = 100 mV s^{-1}, 0.1 M Bu_4NPF_6 as supporting electrolyte, 50% iR compensated). The cyclic voltammogram of compound **7c** was multiplied by factor four for better visibility. b) HOMO and LUMO levels and electrochemical band gaps (solid area) of compounds **7a-c** and **8b,c**.

Electrochemistry. Electrochemical analysis allowed to assess frontier molecular orbitals of these A-π-A molecules. Redox potentials of the compounds were measured by cyclic voltammetry (CV) in CH_2Cl_2 in the presence of Bu_4NPF_6 as a supporting electrolyte and calibrated vs. ferrocenium/ferrocene (Fc^+/Fc). The cyclic voltrammograms are shown in Figure 4a, while the electrochemical properties are summarized in Table 1. Molecule **7a** bearing two dicyanomethylene groups undergoes two reversible reduction processes at −1.00 and −1.25 V. These potentials are comparable to the reduction potentials of a core-unsubstituted perylene bisimide (−0.95, −1.15 V) which was successfully applied as an n-type semiconducting material,[23] and correspond well with the position of the LUMO of fullerenes (−3.8 to −4.3 eV).[24] Furthermore, the reversible reduction processes of indandione derivative **7b** are cathodically shifted vs. potentials of **7a** to −1.12, and −1.49 V, which implies that reduction is more feasible in less electron-rich **7a**. The more pronounced modulation of electron density in A-π-A compounds was achieved upon substitution of the boryl core with strongly electron-accepting DCIND substituents. The first irreversible reduction is located at −0.84 V, followed by several reduction processes which could not be resolved satisfactorily. This is due to a very low solubility of compound **7c** and concomitant low measured currents. Nevertheless, the measurements of redox potentials by more sensitive square-wave voltammetry confirmed the results obtained by CV.

The measurements also show that radical anions of **7a** and **7b** are rather stable, unlike the radical anion of molecule **7c**. In contrast to the impact of the substitution on reduction processes, a variation of the acceptor units has little effect on the oxidation processes. The first oxidation potentials of all A-π-A dyes **7a-c** are observed at comparable values of +0.91, +0.89, and +0.90 V for **7a**, **7b**, and **7c**, respectively, and correspond to irreversible processes. Further oxidation processes were measured at +1.01, +1.17 V for **7b**. The energy levels of FMOs were determined from the CV measurements assuming the energy level of Fc^+/Fc to be at −5.15 eV vs. vacuum.[25] Figure 4b illustrates the band gaps and the positions of the FMOs along with the LUMO level of $PC_{61}BM$ for comparison. The highest occupied molecular orbital (HOMO) levels of A-π-A systems **7a-c** are virtually equal (~ −6.05 eV), while their lowest unoccupied molecular orbitals (LUMOs) vary by 0.28 eV and decrease in the following order: **7b** (−4.03 eV) > **7a** (−4.15 eV) > **7c** (−4.31 eV). Therefore, as demonstrated, we were able to tune significantly the electrochemical behavior of the parent boryl-substituted thienylthiazole via substitution of the core with electron-withdrawing groups. Moreover, low-lying FMO levels indicate high electron affinity of these dyes. The calculated band gaps are in the range of 1.74-2.01 eV, which makes these dyes suitable candidates for solar light harvesters. To evaluate the impact of the boron-bridging on the electrochemical properties of thienylthiazole molecules, we compared the newly synthesized boron complexes with CPDT A-π-A compounds **8b** and **8c** (Scheme 1). The first reduction potentials (and the corresponding LUMO levels, see Figure 4b) of DCIND dyes **7c** and **8c** are equal, whereas the reduction potential of IND derivative **7b** was shifted anodically by 0.18 eV vs. **8b**. This moderate change in LUMO levels has significant consequences on the utilization of indandione derivatives in organic field effect transistors, i.e. **7b** is an n-type, while **8b** a p-type semiconductor.

Quantum chemical calculations. To elucidate the effect of the B-N coordinative bond on the properties of the new systems, we conducted density functional theory (DFT) calculations at the B3LYP[26]/def2-SVP[27] (solvent CH_2Cl_2, PCM model) level of theory for all the synthesized A-π-A molecules. The optimized geometries of dyes **7a-c** and their electrostatic potential maps are displayed in Figure S2. The energies and contour plots of selected Kohn-Sham molecular orbitals, including HOMOs and LUMOs, are illustrated in Figure 5. According to the calculations, all the studied molecules are endowed with essentially planar molecular scaffolds. The HOMOs of **7a-c** are confined to one electron-rich mesityl moiety, while the LUMOs are delocalized over the entire thienylthiazole scaffold and adjacent acceptor units. The next highest occupied molecular orbital (HOMO–1) is composed largely of the π orbital of the second mesityl substituent. Electrostatic potential surfaces show that the electron density is not equally redistributed over the thienylthiazole core pointing that thiazole is more electron poor than a thienyl subunit. Furthermore, indandione derivative features the highest, while malononitrile counterpart – the lowest electron density in the set of synthesized A-π-A systems.

To get insight into the nature of the lowest-energy absorption band we performed TD-DFT calculations (CAM-B3LYP[28]/def2-SVP, solvent CH_2Cl_2, PCM model). The results indicate that $S_0 \rightarrow S_1$ transitions of **7b,c** bearing structurally similar acceptor moieties are mostly attributed to HOMO to LUMO (60-67%) and HOMO–1 to LUMO (18-21%) transitions (Tables S3,S4), which are accompanied by the charge transfer from mesityl substituents to the core with adjacent acceptor units. As suggested by TD-DFT calculations, an experimentally observed broad and irregular absorption band of **7a** in CH_2Cl_2 is a superposition of three transitions and should be ascribed to

10.1002/chem.201701922

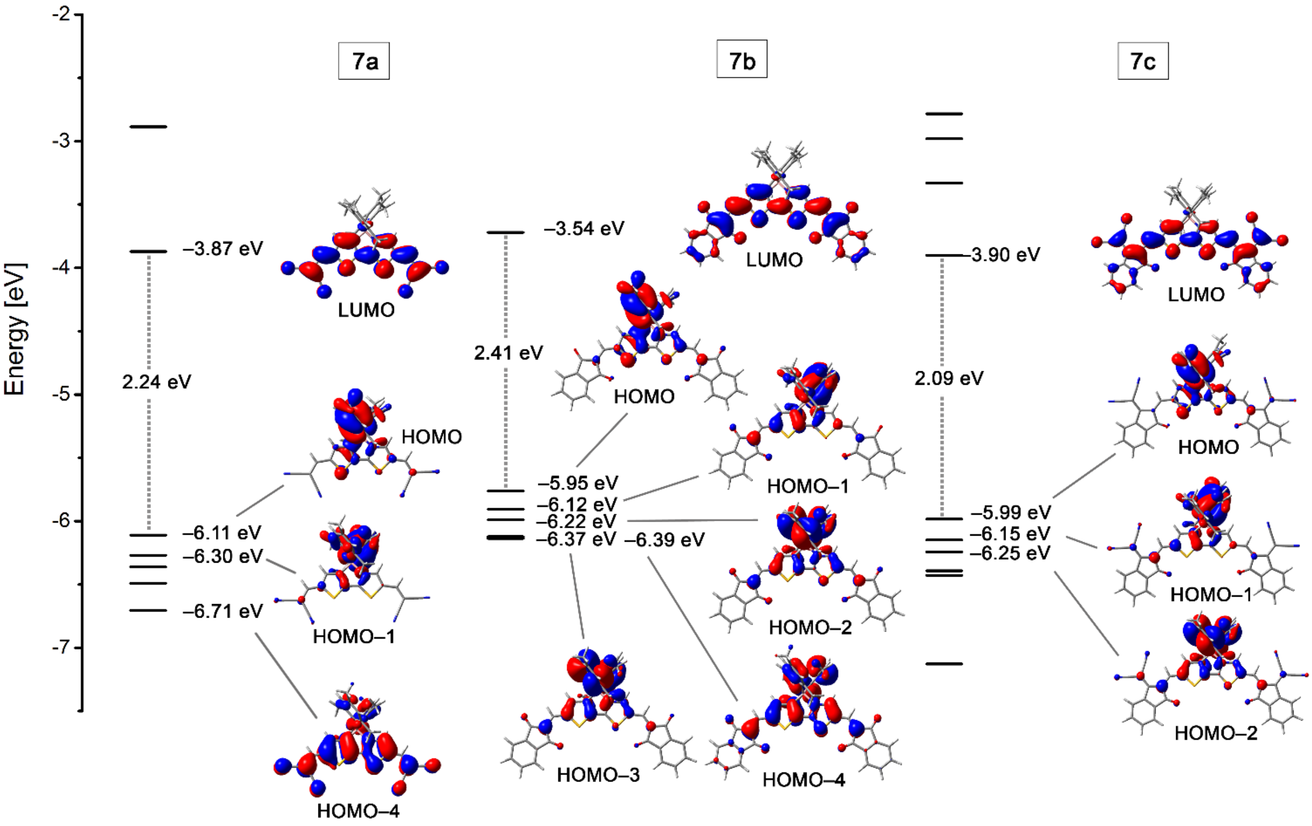

Figure 5. Kohn–Sham orbital energy level diagram of **7a-c** calculated at the B3LYP/def2-SVP (solvent CH_2Cl_2, PCM model) level of theory and contour plots of selected orbitals (isovalue = 0.02 a.u.).

a mixture of mainly HOMO to LUMO, HOMO–1 to LUMO, and HOMO–4 to LUMO transitions (Table S2). In addition to CT from Mes groups to the core, the lowest-energy transition has also some contribution from the π-π* transition of the chelate backbone. The complete TD-DFT data can be found in the Supporting Information.

Device fabrication. To investigate the semiconducting behavior of the new dyes, organic thin film transistor devices (OTFTs) in a bottom-gate, top-contact configuration were prepared by vacuum deposition of the organic materials on $Si/SiO_2/AlO_x$ substrates, covered with a monolayer of *n*-tetradecylphosphonic acid (TPA). The devices had a channel length *L* of 100 μm and a channel width *W* of 200 μm, defined by gold contacts. The OTFTs were characterized by measuring transfer and output curves under ambient conditions. The charge carrier mobility *μ* was estimated according to the following equation: $\mu = 2\, I_{DS}\, L/[W\, C_i(V_{GS} - V_T)^2]$, where I_{DS} describes the drain-source current, C_i the capacitance of the gate dielectric, V_{GS} denotes the gate-source voltage, V_T the threshold voltage and *L* and *W* are defined as transistor channel length and width, respectively. Thermal properties of **7a-c** were investigated by differential scanning calorimetry (DSC). DSC curves for **7a** and **7b** indicate that these compounds are stable until melting at 230.3 and 268.8 °C, respectively, whereas **7c** is robust up to ~ 350°C and does not show any isotropization peak (Figure S6). Thus, the boron compounds **7a-c** exhibit high thermal stability and are suitable for vacuum deposition. When **7a**, featuring a small π-scaffold, was used as an active material, the OTFTs did not work. Conversely, compounds **7b** and **7c**, whose chromophores are much more extended by the IND or DCIND acceptors, showed semiconducting n-type behavior. Electron mobility of 5.55×10^{-4} cm^2 V^{-1} s^{-1} [$\mu_{max} = 6.05 \times 10^{-4}$ cm^2 V^{-1} s^{-1}], a current on/off ratio of 4 × 10^3 and a threshold voltage of +1 V could be measured for the devices based on molecule **7b**. Even better electron mobility as high as 1.39×10^{-2} cm^2 V^{-1} s^{-1} [$\mu_{max} = 1.56 \times 10^{-2}$ cm^2 V^{-1} s^{-1}], an on/off ratio of 2 ×10^6 and a V_T of +6 V were measured for devices with compound **7c**. The transfer curves and square root plots of the drain-source current of devices based on **7b** and **7c** are shown in Figure 6a. Both yielded transfer curves with significant hystereses.

The atomic force microscopy images of the corresponding devices (Figure 6b and c) show that **7b** exhibits a densely packed and uniform surface morphology, while the thin film of **7c** shows much more defined structures, indicating a higher crystallinity.

At the microscopic scale, the efficiency of charge transport in organic semiconductors is determined by two key parameters, i.e. the electronic coupling (transfer integral) between adjacent molecules and the reorganization energy (*λ*). The charge carrier mobility is higher if the first factor is maximized and when *λ* is as small as possible. To rationalize the observed differences in electron mobility of the new A-π-A molecules, we calculated the inner-sphere reorganization energy (λ_i) (for details, see the Supporting Information). The obtained λ_i values for the molecules

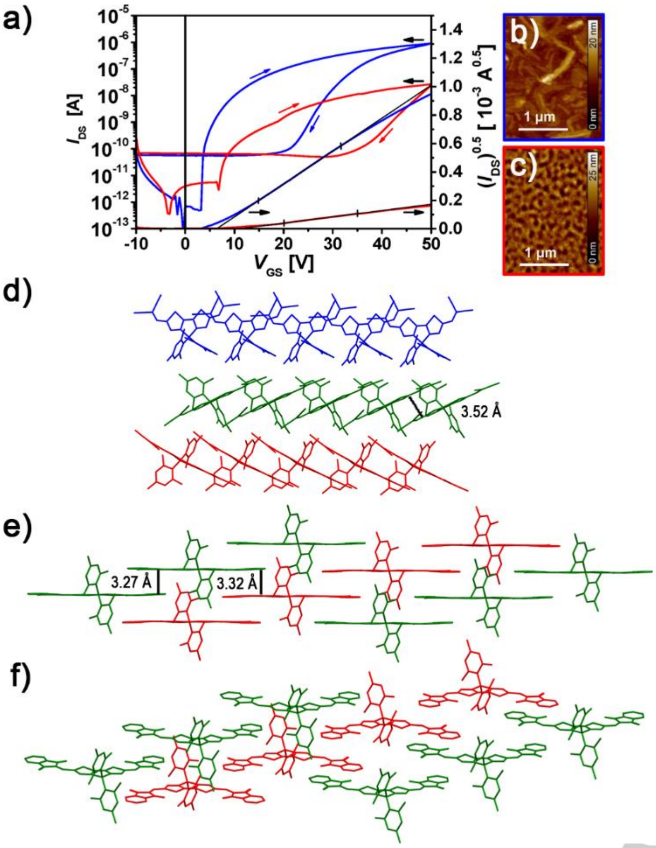

Figure 6. a) Transfer curves and square root plots of the drain-source current with corresponding linear fit (black line) for OTFT devices based on molecule **7b** (red) and **7c** (blue). The black arrows are indicating the relevant y-axis. Devices were prepared on TPA-modified substrates and measured under ambient conditions. AFM morphology measured between the contacts of the corresponding devices of molecules b) **7c**, and c) **7b**. The packing arrangement of d) **7a**, and e) and f) **7b**. Solvent molecules and hydrogen atoms are omitted for clarity.

increase in the following order: **7c** (0.235 eV) < **7a** (0.266 eV) < **7b** (0.307 eV). **7c** features the smallest reorganization energy and shows the highest electron mobility. For comparison, the reported λ_i for the common electron transport material Alq_3 is 0.276 eV.[29] The reorganization energy of the malononitrile derivative is smaller than that of **7b**. However, the devices employing **7a** as an active layer did not show any charge transport behavior, in contrast to the devices based on **7b**. These results indicate an important role of the packing arrangement and intramolecular interactions between adjacent molecules.

The steric hindrance of the bulky mesityl groups in combination with the small size of the π-scaffold in molecule **7a** could prevent a close π-stacking and a good orbital overlap between the molecules. In the packing arrangement of derivative **7a** only one-dimensional stacks are observed. The molecules are aligned parallel with the interplanar distance of 3.52 Å in a slipped arrangement (Figure 6d). This alignment is governed by the bulkiness of mesityl group and electrostatic interactions between electron-rich thiophene ring and a dicyanomethylene group of adjacent molecule, i.e. a short contact of 3.41 Å is observed between sp^2 carbon atom of $C(CN)_2$ and sulfur thiophene atom of a neighboring molecule. Due to lack of π-overlaps, interactions between adjacent molecules are effectively diminished.

We rationalize a better performance of molecules **7b** and **7c** in OTFT devices by the increased interchromophoric interactions imparted by the acceptor units with an extended π-surface. The behavior of **7b** can be related to its packing arrangement. In contrast to crystals of **7a**, crystals of **7b** include solvent molecules (i.e. 2.5 molecules of toluene per one molecule of **7b**). Nevertheless, it is clear that **7b** shows a tendency to pack in a two-dimensional (2D) layer structure. In the molecular packing structure, the molecules are arranged in a slipped fashion in a 2D array. That is, parallel-oriented molecules (red color in Figure 6e,f) form one-dimensional stacks with the interplanar distances of 3.27 Å. The distance between mean planes of antiparallel-oriented molecules (red and green color in Figure 6e,f) is 3.32 Å. An acceptor moiety of one molecule is located partially over a vinylene bridge and an acceptor moiety of an adjacent molecule, which results in effective π-orbital overlaps (short contacts 3.34-3.39 Å). These stacks are interacting with neighboring arrays of antiparallel-oriented molecules via C-H···π interactions between indandione C-H and mesityl π-surface, as well as π-π interactions between thiophene ring and a vinylene bridge of one molecule with an acceptor moiety of an adjacent molecule (short contacts of 3.34-3.38 Å), and interaction between acceptor units of both molecules with antiparallel orientation (short contacts of 3.36 Å). Thus, there is an evident communication between neighboring layers.

Importantly, both **7b** and **7c** display n-type semiconducting behavior, whereas in the structurally related CPDT the charge-transport behavior is dependent on the type of acceptor moieties. These results evidence that the strategy based on a) achieving low LUMO energy levels by applying a boron-bridge combined with b) the extension of the π-scaffolds by a certain type of acceptor units proved an effective way to obtain n-type semiconducting materials. In particular, dye **7c** with mobility ca. 1.4 × 10^{-2} cm^2 V^{-1} s^{-1} constitutes a potential candidate for further applications in vacuum processed organic solar cells, e.g. for replacement of fullerene acceptors.[30] It is worth noting that electron mobilities of organoboron small molecules reported to date for OFET devices[12,31] or obtained from time-of-flight (TOF) carrier-mobility measurements[17,32] are usually at least 10 times lower than electron mobility observed for **7c**. A further increase in mobility can be most probably achieved upon replacement of mesityl groups with less sterically demanding substituents on the boron center and extension of the core.

Conclusions

The newly synthesized A-π-A molecules display attractive properties along with exceptional stability. We showed that by a gradual increase in the acceptor strength from IND to DCIND we were able to systematically lower LUMO levels of the boron-bridged A-π-A dyes. A variation of acceptor substituents in combination with a B-N motive in the central π-core afforded promising molecules with low band gaps and LUMO levels comparable to $PC_{61}BMs$ LUMO level. To demonstrate the promising features of A-π-A molecules for organic electronics, thin film transistors were fabricated. OFET devices using **7c** as a semiconducting layer were found to exhibit electron mobility under ambient conditions of ca. 1.4 × 10^{-2} cm^2 V^{-1} s^{-1}, which is the highest value reported to date for organoboron small molecules. The superior behavior of DCIND and IND derivatives

10.1002/chem.201701922

to a malononitrile derivative can be attributed to a 2D packing arrangement and stronger interchromophoric interactions which are effectively enhanced by the presence of the acceptor units with an extended π-surface. Moreover, a comparison of boron-bridging with carbon-bridging in structurally related indandione derivatives indicates that incorporation of boron into an aromatic scaffold is an effective way towards n-channel materials.

Experimental Section

Experimental.

General. All reagents were purchased from commercial sources and used as received without further purification, unless otherwise stated. Reagent grade solvents were distilled prior to use. Column chromatography was performed on silica (silica gel, 230–400 mesh). ^{1}H, ^{13}C, ^{11}B NMR, and 2D NMR spectra were recorded on a Bruker Avance 400 spectrometer or a Bruker DMX 600 spectrometer ^{1}H, and ^{13}C NMR spectra were calibrated to the residual solvent signals. ^{11}B NMR spectra were calibrated to the signal of boron trifluoride diethyl etherate ($BF_3{\cdot}OEt_2$) as external standard. *J* values are given in Hz. The following abbreviations were used to designate multiplicities: s = singlet, d = doublet, t = triplet, m = multiplet. High resolution mass spectra were obtained by electrospray ionization (ESI) and were recorded on an ESI micrOTOF Focus spectrometer from Bruker Daltonics. Low resolution mass spectra were obtained by matrix-assisted laser desorption/ionisation (MALDI) and were recorded on an Autoflex II MALDI-TOF mass spectrometer (Bruker Daltonik GmbH). Melting points were determined on an optical microscope and are uncorrected. Malononitrile (**6a**) and 1,3-indandione (**6b**) were commercially available. Compounds **1**[21] and **2**,[22] and **6c**[33] were prepared according to the reported procedures.

UV/Vis absorption and fluorescence spectroscopy. UV/Vis absorption measurements were performed using Lambda 950 (Perkin-Elmer) or Jasco V-670 including NCP-706 thermostatted 6-position automatic cell changer. The spectra were measured in spectroscopic grade solvents from ACROS at a concentration of about 10^{-6} - 10^{-5} M^{-1} in quartz cuvettes with path lengths of 1 cm at room temperature. Fluorescence was investigated on a QM-4/2003 (PTI) by the optical dilution method (OD < 0.05).[34]

Electrochemical analysis. The CV measurements were performed on a standard, commercial electrochemical analyzer (EC epsilon; BAS Instruments, UK) in a three electrode single-compartment cell under an argon atmosphere. Dichloromethane (HPLC grade) was dried over calcium hydride under an argon atmosphere, distilled, and degassed prior to use. The supporting electrolyte NBu_4PF_6 was synthesized according to the literature,[35] recrystallized from ethanol/water, and dried in a high vacuum. The measurements were carried out in dichloromethane/0.1 M NBu_4PF_6 under the exclusion of air and moisture at a concentration of $2.5 \times 10^{-4} - 1.1 \times 10^{-3}$ M with the ferrocenium/ferrocene redox couple (−5.15 eV vs. vacuum)[25] as an internal standard for the calibration of the potential. A cyclic voltammogram of **7c** was measured at a lower concentration due to the low solubility of the compound. Working electrode: Pt disc (Ø 3 mm); reference electrode: Ag/AgCl; auxiliary electrode: Pt wire. The internal resistance was compensated by 50 %.

Synthetic procedures and product characterization

Synthesis of compound 5. A solution of compound **4** (300 mg; 0.72 mmol) in dry THF (7.2 ml) was cooled to –78 °C and *n*BuLi (2.5 M in hexane; 0.66 mL; 1.65 mmol) was added dropwise. The reaction mixture was stirred at –78 °C for 1 h. Then dry DMF (0.17 ml; 2.20 mmol) was added dropwise and the stirring was continued at –78 °C. After 40 min the mixture was allowed to warm to RT and stirred at this temperature for the next 1.5 h. Afterwards, the reaction was quenched with a saturated aqueous solution of NH_4Cl. A water layer was extracted with CH_2Cl_2, dried over Na_2SO_4, filtered and evaporated. The crude product was purified by column chromatography (silica; pentane/EtOAc 9:1) and crystallized (EtOAc/pentane) to give **5** (225 mg, 66%) as orange crystals. M.p. 215-218 °C (EtOAc/pentane). ^{1}H NMR (400 MHz, $CDCl_3$, 25 °C) δ 9.96 (s, 1H), 9.90 (s, 1H), 8.32 (s, 1H), 7.87 (s, 1H), 6.70 (s, 4H), 2.20 (s, 6H), 1.87 (s, 12H). ^{13}C NMR (100 MHz, $CDCl_3$, 25 °C) δ 184.4, 180.6, 170.2, 152.7, 145.2, 140.1, 138.8, 138.7, 135.8, 135.5, 130.1, 24.6, 20.9 (two carbon signals corresponding to the C atoms bound to the B atom are not visible due to the quadrupolar relaxation). MS HR (ESI) *m*/*z* calcd for $C_{27}H_{26}BNNaO_2S_2$ $[M+Na]^+$ 494.1390, found 494.1386. Anal. calcd for $C_{27}H_{26}BNO_2S_2$: C, 68.79, H, 5.56, N, 2.97, S, 13.60. Found: C, 68.71, H, 5.69, N, 2.92, S, 13.69.

Synthesis of compound 7a. To dialdehyde **5** (100 mg, 0.21 mmol) and compound **6a** (56 mg, 0.85 mmol) in dichloroethane (8 mL) dry pyridine (0.17 mL, 2.11 mmol) was added and the reaction mixture was stirred at 60 °C for 1 h 45 min. Then the solution was loaded on a column and chromatographed (silica, CH_2Cl_2). The consecutive chromatography (silica CH_2Cl_2/pentane 4:1) afforded pure **7a** which was recrystallized (CH_2Cl_2/pentane) to give **7a** (92 mg, 77%) as a red solid. ^{1}H NMR (400 MHz, CD_2Cl_2, 25 °C) δ 8.23 (d, *J* = 0.5 Hz, 1H), 7.91 (d, *J* = 0.5 Hz, 1H), 7.86 (d, *J* = 0.5 Hz, 1H), 7.71 (d, *J* = 0.5 Hz, 1H), 6.69 (s, 4H), 2.18 (s, 6H), 1.86 (s, 12H). ^{13}C NMR (101 MHz, CD_2Cl_2, 25 °C) δ 168.6, 151.7, 148.2, 148.1, 144.6, 142.3, 140.6, 139.8, 136.8, 131.8, 130.4, 113.9, 113.4, 113.0 112.8, 83.3, 81.9, 24.6, 21.1 (two carbon signals corresponding to the C atoms bound to the B atom are not visible due to the quadrupolar relaxation). ^{11}B NMR (128 MHz, CD_2Cl_2, 25 °C) δ 3.24. UV/Vis (CH_2Cl_2, *c* = 6.89×10^{-5} M): λ_{max}/nm 454 (ε/M^{-1} cm^{-1} 35 000), 325 (17 000). MS LR (MALDI) *m*/*z* calcd for $C_{33}H_{26}BN_5S_2$ M^- 567.2 found 567.1. MS HR (ESI) *m*/*z* calcd for $C_{33}H_{26}BN_5S_2$ M^- 567.1723, found 567.1609. MS HR (ESI) *m*/*z* calcd for $C_{24}H_{15}BN_5S_2$ $[M-Mes]^+$ 448.0856, found 448.0873.

Synthesis of compounds 7b. To dialdehyde **5** (100 mg, 0.21 mmol) and compound **6b** (124 mg, 0.85 mmol) in dichloroethane (8 mL) dry pyridine (0.17 mL, 2.11 mmol) was added and the reaction mixture was stirred at 60 °C for 2.5 h. Then the solution was loaded on a column and chromatographed (silica, CH_2Cl_2) to give product **7b** which was crystallized (CH_2Cl_2/pentane) to give pure **7b** (81 mg, 53%) as a dark red solid. ^{1}H NMR (400 MHz, CD_2Cl_2, 25 °C) δ 9.89 (s, 1H), 8.31 (s, 1H), 7.98–7.88 (m, 2H), 7.83–7.77 (m, 3H), 7.75 (s, 1H), 6.59 (s, 4H), 2.09 (s, 6H), 1.79 (s, 12H). ^{13}C NMR (101 MHz, CD_2Cl_2, 25 °C) δ 190.3, 189.83, 189.76, 188.8, 171.2, 149.0, 148.0, 144.3, 142.8, 142.4, 141.4, 141.2, 140.6, 140.4, 136.5 136.4, 136.1, 136.0, 135.9, 135.1, 132.9, 131.5, 130.4, 128.1, 127.6, 124.99, 123.96, 123.7, 24.9, 21.0 (two carbon signals corresponding to the C atoms bound to the B atom are not visible due to the quadrupolar relaxation). ^{11}B NMR (128 MHz, CD_2Cl_2, 25 °C) δ 5.17. UV/Vis (CH_2Cl_2, *c* = 1.02×10^{-5} M): λ_{max}/nm 530 (ε/M^{-1} cm^{-1} 56 000), 493 (54 000), 361 (21 00) with two shoulders. MS HR (ESI) m/z calcd for $C_{45}H_{35}BNO_4S_2$ $[M+H]^+$ 728.2095, found 728.2087.

Synthesis of compound 7c. The flask was charged with compound **5** (100.0 mg; 0.21 mmol) and CH-acid **6c** (165 mg; 0.85 mmol). Then DCE (8 mL) and pyridine (0.17 ml; 2.11 mmol) were added and the reaction mixture was stirred at 60 °C for 2 h. Afterwards, the reaction was cooled to RT and the precipitate was filtered and washed with acetone (150 mL). The resulting solid was suspended in the mixture of acetone and pentane and filtered to give **7c** (130 mg, 74%) as dark purple crystals. ^{1}H NMR (400 MHz, $C_2D_2Cl_4$, 125 °C) δ 8.86 (s, 1H), 8.83–8.74 (m, 2H), 8.72 (s, 1H), 8.37 (s, 1H), 8.07 (t, *J* = 5.9 Hz, 2H), 7.97–7.77 (m, 5H), 6.76 (s, 4H), 2.27 (s, 6H), 2.06 (s, 12H). ^{1}H NMR (600 MHz, $C_2D_2Cl_4$, 75 °C) δ 8.88 (s, 1H), 8.82–8.64 (m, 3H), 8.42–8.29 (m, 1H), 8.14–7.99 (m, 2H), 7.97–7.78 (m, 5H), 6.72 (s, 4H), 2.24 (s, 6H), 1.95 (s, 12H). ^{13}C NMR (151 MHz, CD_2Cl_2, 75 °C) δ 188.0, 187.5, 170.8, 159.5, 158.2, 151.4, 146.5, 145.4, 143.9, 141.0, 140.1, 137.2, 136.9, 136.5, 136.2, 135.5, 135.2, 134.9, 133.0, 132.4, 129.6, 126.5, 125.5, 125.3, 124.5, 124.2, 123.6, 120.2, 113.9, 113.4, 99.5, 79.7, 79.5, 79.4, 24.0, 20.7 (two carbon signals corresponding to the C atoms bound to the B atom are not visible due to the quadrupolar relaxation). Compound **7c** features very low solubility. ^{1}H NMR spectra were measured at 125 °C and 75 °C. The measurement at 125 °C shows sharper proton signals. However, the ^{13}C NMR spectrum could not be collected at such a high temperature because a sample partially decomposed during the required long acquisition time. ^{11}B NMR (128 MHz, CD_2Cl_2, 25 °C) δ 3.89. UV/Vis (CH_2Cl_2, c = 4.10 × 10^{-6} M): λ_{max}/nm 589 (ε/M^{-1} cm^{-1} 67 000), 554 (62 000), 305 (43 000) with two shoulders. MS LR (MALDI) *m/z* calcd for $C_{51}H_{34}BN_5O_2S_2$ M^+ 823.2, found 823.2. MS HR (ESI) m/z calcd for $C_{51}H_{35}BN_5O_2S_2$ $[M+H]^+$ 824.2320, found 824.2319.

Acknowledgements

We are grateful to Prof. Frank Würthner for his support and many helpful discussions. We would like to thank Christian Simon for the technical assistance in the synthesis of the building blocks. We thank the Bavarian State Ministry of Education, Science, and the Arts for financial support of this project by the establishment of the Key Laboratory "Supramolecular Polymers" at the Bavarian Polymer Institute (BPI) and the University of Würzburg for support by the Emil Hilb Program.

Keywords: boron • OTFT • A-π-A molecules • electron transport • thienylthiazole

[1] a) C. D. Entwistle, T. B. Marder, *Angew. Chem. Int. Ed.* **2002**, *41*, 2927-2931; *Angew. Chem.* **2002**, *114*, 3051-3056; b) C. D. Entwistle, T. B. Marder, *Chem. Mater.* **2004**, *16*, 4574-4585; c) S. Yamaguchi, A. Wakamiya, *Pure Appl. Chem.* **2006**, *78*, 1413-1424 d) F. Jäkle, *Chem. Rev.* **2010**, *110*, 3985-4022; e) A. Lorbach, A. Hübner, M. Wagner, *Dalton Trans.* **2012**, *41*, 6048-6063; f) X. Y. Wang, J. Y. Wang, J. Pei, *Chem. Eur. J.* **2015**, *21*, 3528-3539; g) Y. Ren, F. Jäkle, *Dalton Trans.* **2016**, *45*, 13996-14007; h) A. Wakamiya, S. Yamaguchi, *Bull. Chem. Soc. Jpn.* **2015**, *88*, 1357-1377; i) D. L. Crossley, I. Vitorica-Yrezabal, M. J. Humphries, M. L. Turner, M. J. Ingleson, *Chem. Eur. J.* **2016**, *22*, 12439-12448; j) M. Grandl, B. Rudolf, Y. Sun, D. F. Bechtel, A. J. Pierik, F. Pammer, *Organometallics* **2017**, DOI:10.1021/acs.organomet.6b00916.

[2] a) D. Li, H. Zhang, Y. Wang, *Chem. Soc. Rev.* **2013**, *42*, 8416-8433 and references therein. For some more recent reports see: b) H.-W. Mo , Y. Tsuchiya, Y. Geng, T. Sagawa, C. Kikuchi, H. Nakanotani, F. Ito, C. Adachi, *Adv. Funct. Mater.* **2016**, *26*, 6703-6710; c) B. Y.-W. Wong, H.-L. Wong, Y.-C. Wong, M.-Y. Chan, V. W.-W. Yam, *Chem. Eur. J.* **2016**, *22*, 15095-15106; d) Y.-J. Shiu, Y.-C. Cheng, W.-L. Tsai, C.-C. Wu, C.-T. Chao, C.-W. Lu, Y. Chi, Y.-T. Chen, S.-H. Liu, P.-T. Chou, *Angew. Chem. Int. Ed.* **2016**, *55*, 3017-3021; *Angew. Chem.* **2016**, *128*, 3069-3073; e) S. Wang, D.-T. Yang, J. Lu, H. Shimogawa, S. Gong, X. Wang, S. K. Mellerup, A. Wakamiya, Y.-L. Chang, C. Yang, Z.-H. Lu, *Angew. Chem. Int. Ed.* **2015**, *54*, 15074-15078; *Angew. Chem.* **2015**, *127*, 15289-15293; f) K. Suzuki, S. Kubo, K. Shizu, T. Fukushima, A. Wakamiya, Y. Murata, C. Adachi, H. Kaji, *Angew. Chem. Int. Ed.* **2015**, *54*, 15231-15235; *Angew. Chem.* **2015**, *127*, 15446-15450.

[3] A. J. C. Kuehne, M. C. Gather, *Chem. Rev.* **2016**, *116*, 12823-12864.

[4] a) J. M. Hales, S. Barlow, H. Kim, S. Mukhopadhyay, J. L. Bredas, J. W. Perry, S. R. Marder, *Chem. Mater.* **2014**, *26*, 549-560; b) L. Ji, R. M. Edkins, L. J. Sewell, A. Beeby, A. S. Batsanov, K. Fucke, M. Drafz, J. A. K. Howard, O. Moutounet, F. Ibersiene, A. Boucekkine, E. Furet, Z. Liu, J.-F. Halet, C. Katan, T. B. Marder, *Chem. Eur. J.* **2014**, *20*, 13618-13635; c) J. C. Collings, S.-Y. Poon, C. Le Droumaguet, M. Charlot, C. Katan, L.-O. Pålsson, A. Beeby, J. A. Mosely, H. M. Kaiser, D. Kaufmann, W.-Y. Wong, M. Blanchard-Desce, T. B. Marder, *Chem. Eur. J.* **2009**, *15*, 198-208; d) A. Hayek, J.-F. Nicoud, F. Bolze, C. Bourgogne, P. L. Baldeck, *Angew. Chem. Int. Ed.* **2006**, *45*, 6466-6469; *Angew. Chem.* **2006**, *118*, 6616-6619.

[5] a) S. Griesbeck, Z. Zhang, M. Gutmann, T. Lehmann, R. M. Edkins, G. Clermont, A. N. Lazar, M. Haehnel, K. Edkins, A. Eichhorn, M. Blanchard-Desce, L. Meinel, T. B. Marder, *Chem. Eur. J.* **2016**, *22*, 14701-14706; b) X. Li, X. Guo, L. Cao, Z. Xun, S. Wang, S. Li, Y. Li, G. Yang, *Angew. Chem. Int. Ed.* **2014**, *53*, 7809-7813; *Angew. Chem.* **2014**, *126*, 7943-7947; c) G. M. Fischer, C. Jüngst, Magnus Isomäki-Krondahl, D. Gauss, H. M. Möller, E. Daltrozzo, A. Zumbusch, *Chem. Commun.*, **2010**, *46*, 5289-5291; d) V. F. Pais, M. M. Alcaide, R. López-Rodriguez, D. Collado, F. Nájera, E. Pérez-Inestrosa, E. Álvarez, J. M. Lassaletta, R. Fernández, A. Ros, U. Pischel, *Chem. Eur. J.* **2015**, *21*, 15369-15376; e) S. V. Mulay, T. Yudhistira, M. Choi, Y. Kim, J. Kim, Y. J. Jang, S. Jon, D. G. Churchill, *Chem. Asian J.* **2016**, *11*, 3598-3605.

[6] Y.-L. Rao, H. Amarne, S. Wang, *Coord. Chem. Rev.* **2012**, *256*, 759-770.

[7] a) Y. L. Chang, Y. L. Rao, S. Gong, G. L. Ingram, S. Wang, Z. H. Lu, *Adv. Mater.* **2014**, *26*, 6729-6733; b) C. T. Poon, D. Wu, W. H. Lam, V. W. W. Yam, *Angew. Chem. Int. Ed.* **2015**, *54*, 10569-10573; *Angew. Chem.* **2015**, *127*, 10715-10719; c) C. T. Poon, D. Wu, V. W. W. Yam, *Angew. Chem. Int. Ed.* **2016**, *55*, 3647-3651; *Angew. Chem.* **2016**, *128*, 3711-3715.

[8] a) C.-W. Chiu, Y. Kim, F. P. Gabbaï, *J. Am. Chem. Soc.* **2009**, *131*, 60-61; b) Y. Kim, F. P. Gabbaï, *J. Am. Chem. Soc.* **2009**, *131*, 3363-3369; c) T. Agou, M. Sekine, J. Kobayashi, T. Kawashima, *Chem. Eur. J.* **2009**, *15*, 5056-5062; c) K. C. Song, K. M. Lee, N. V. Nghia, W. Y. Sung, Y. Do, M. H. Lee, *Organometallics* **2013**, *32*, 817-823, d) Z. Zhang, R. M. Edkins J. Nitsch, K. Fucke, A. Eichhorn, A. Steffen, Y. Wang, T. B. Marder, *Chem. Eur. J.* **2015**, *21*, 177-190; e) S. K. Sarkar, S. Mukherjee, P. Thilagar, *Inorg. Chem.* **2014**, *53*, 2343-2345.

[9] a) A. E. Ashley, T. J. Herrington, G. G. Wildgoose, H. Zaher, A. L. Thompson, N. H. Rees, T. Krämer, D. O'Hare, *J. Am. Chem. Soc.* **2011**, *133*, 14727-14740; b) H. Braunschweig, A. Damme, J. O. C. Jimenez-Halla, C. Hörl, I. Krummenacher, T. Kupfer, L. Mailänder, K. Radacki, *J. Am. Chem. Soc.* **2012**, *134*, 20169-20177.

[10] a) S. Yamaguchi, T. Shirasaka, S. Akiyama, K. Tamao, *J. Am. Chem. Soc.* **2002**, *124*, 8816-8817. b) A. Caruso, Jr., M. A. Siegler, J. D. Tovar, *Angew. Chem. Int. Ed.* **2010**, *49*, 4213-4217; *Angew. Chem.* **2010**, *122*, 4309-4313; c) Z. Zhang, R. M. Edkins, J. Nitsch, K. Fucke, A. Steffen, L. E. Longobardi, D. W. Stephan, C. Lambert, T. B. Marder, *Chem. Sci.* **2015**, *6*, 308-321; d) X. Yin, J. Chen, R. A. Lalancette, T. B. Marder, F. Jäkle, *Angew. Chem. Int. Ed.* **2014**, *53*, 9761-9765; *Angew. Chem.* **2014**, *126*, 9919-9923.

[11] e.g. a) Z. Zhou, A. Wakamiya, T. Kushida, S. Yamaguchi, *J. Am. Chem. Soc.* **2012**, *134*, 4529-4532; b) S. Saito, K. Matsuo, S. Yamaguchi, *J. Am. Chem. Soc.* **2012**, *134*, 9130-9133; c) T. Kushida, A. Shuto, M. Yoshio, T. Kato, S. Yamaguchi, *Angew. Chem. Int. Ed.* **2015**, *54*, 6922-6925; *Angew. Chem.* **2015**, *127*, 7026-7029; d) K. Matsuo, S. Saito, S. Yamaguchi, *Angew. Chem. Int. Ed.* **2016**, *55*, 11984-11988; *Angew. Chem.* **2016**, *128*, 12163-12167; e) K. Schickedanz, T. Trageser, M. Bolte, H.-W. Lerner, M. Wagner, *Chem. Commun.* **2015**, *51*, 15808-15810; f) T. Hatakeyama, K. Shiren, K. Nakajima, S. Nomura, S. Nakatsuka, K. Kinoshita, J. Ni, Y. Ono, T. Ikuta, *Adv. Mater.* **2016**, *28*, 2777-2781; g) Y. Kitamoto, T. Suzuki, Y. Miyata, H. Kita, K. Funakid, S. Oi, *Chem. Commun.* **2016**, *52*, 7098-7101.

[12] K. Ono, A. Nakashima, Y. Tsuji, T. Kinoshita, M. Tomura, J.-i. Nishida, Y. Yamashita, *Chem. Eur. J.* **2010**, *16*, 13539-13546.

[13] H. Shimogawa, O. Yoshikawa, Y. Aramaki, M. Murata, A. Wakamiya, Y. Murata, *Chem. Eur. J.* **2017**, *23*, 3784-3791.

[14] *Molecular Probes™ Handbook. A Guide to Fluorescent Probes and Labeling Technologies*, 11th Ed. **2010**.

[15] http://www.cyanagen.com, **2017**.

[16] A. Nowak-Król, R. Wagener, F. Kraus, A. Mishra, P. Bäuerle, F. Würthner, *Org. Chem. Front.* **2016**, *3*, 545-555.

[17] A. Wakamiya, T. Taniguchi, S. Yamaguchi, *Angew. Chem. Int. Ed.* **2006**, *45*, 3170-3173; *Angew. Chem.* **2006**, *118*, 3242-3245.

[18] a) C. Dou, Z. Ding, Z. Zhang, Z. Xie, J. Liu, L. Wang, *Angew. Chem. Int. Ed.* **2015**, *54*, 3648-3652; *Angew. Chem.* **2015**, *127*, 3719-3723; b) R. Zhao, C. Dou, Z. Xie, J. Liu, L. Wang, *Angew. Chem. Int. Ed.* **2016**, *55*, 5313-5317; *Angew. Chem.* **2016**, *128*, 5399-5403.

[19] a) H. Shimogawa, M. Endo, T. Taniguchi, Y. Nakaike, M. Kawaraya, H. Segawa, Y. Murata, A. Wakamiya, *Bull. Chem. Soc. Jpn.* **2017**, *90*, 441-450; b) H. Shimogawa, M. Endo, Y. Nakaike, Y. Murata, A. Wakamiya, *Chem. Lett.* **2017**, *46*, 715-718.

[20] a) N. M. Kronenberg, M. Deppisch, F. Würthner, H. W. A. Lademann, K. Deing, K. Meerholz, *Chem. Commun.* **2008**, 6489-6491; b) H. Bürckstümmer, E. V. Tulyakova, M. Deppisch, M. R. Lenze, N. M. Kronenberg, M. Gsänger, M. Stolte, K. Meerholz, F. Würthner, *Angew. Chem. Int. Ed.* **2011**, *50*, 11628-11632; *Angew. Chem.* **2011**, *123*, 11832-11836; c) A. Arjona-Esteban, J. Krumrain, A. Liess, M. Stolte, L. Huang, D. Schmidt, V. Stepanenko, M. Gsänger, D. Hertel, K. Meerholz, F. Würthner, *J. Am. Chem. Soc.* **2015**, *137*, 13524-13534.

[21] A. C. J. Heinrich, B. Thiedemann, P. J. Gates, A. Staubitz, *Org. Lett.* **2013**, *15*, 4666-4669.

[22] S. Pu, C. Zheng, Q. Sun, G. Liu, C. Fan, *Chem. Commun.* **2013**, *49*, 8036-8038.

[23] R. Schmidt, J. H. Oh, Y.-S. Sun, M. Deppisch, A.-M. Krause, K. Radacki, H. Braunschweig, M. Könemann, P. Erk, Z. Bao, F. Würthner, *J. Am. Chem. Soc.* **2009**, *131*, 6215-6228.

[24] These values correspond to reduction potentials E^{red} of −1.04 and −0.85 V (the values vary due to to different measurement conditions and calibration procedures): a) C.-Z. Li, H.-L. Yip, A. K.-Y. Jen, *J. Mater. Chem.* **2012**, *22*, 4161-4177; b) M .C. Scharber, D. Mühlbacher, M. Koppe, P. Denk, C. Waldauf, A. J. Heeger, C. J. Brabec, *Adv. Mater.* **2006**, *18*, 789-794; c) C.-P- Chen, Y.-W. Lin, J.-C. Horng, S.-C. Chuang, *Adv. Energy Mater.* **2011**, *1*, 776-780.

[25] a) N. G. Connelly, W. E. Geiger, *Chem. Rev.* **1996**, *96*, 877-910; b) W. N. Hansen, G. J. Hansen, *Phys. Rev. A* **1987**, *36*, 1396-1402; c) C. M. Cardona, W. Li, A. E. Kaifer, D. Stockdale, G. C. Bazan, *Adv. Mater.* **2011**, *23*, 2367-2371.

[26] a) A. D. Becke, *Phys. Rev. A* **1988**, *38*, 3098-3100; b) C. Lee, W. Yang, R. G. Parr, *Phys. Rev. B* **1988**, *37*, 785-789; c) A. D. Becke, *J. Chem. Phys.* **1993**, *98*, 5648-5652.

[27] F. Weigend, R. Ahlrichs, *Phys. Chem. Chem. Phys.* **2005**, *7*, 3297-3305.

[28] T. Yanai, D. Tew, N. Handy, *Chem. Phys. Lett.* **2004**, 393, 51-57.

[29] B. C. Lin, C. P. Cheng, Z.-Q. You, C.-P. Hsu, *J. Am. Chem. Soc.* **2005**, *127*, 66-67.

[30] a) S. Li, Z. Zhang, M. Shi, C.-Z. Li, H. Chen, *Phys. Chem. Chem. Phys.* **2017**, *19*, 3440-3458; b) W. Chen, Q. Zhang, *J. Mater. Chem. C* **2017**, *5*, 1275-1302.

[31] a) T. Bura, N. Leclerc, S. Fall, P. Lévêque, T. Heiser, P. Retailleau, S. Rihn, A. Mirloup, R. Ziessel, *J. Am. Chem. Soc.* **2012**, *134*, 17404-17407; b) K. Matsuo, S. Saito, S. Yamaguchi, *J. Am. Chem. Soc.* **2014**, *136*, 12580-12583.

[32] a) D. Li, Y. Yuan, H. Bi, D. Yao, X. Zhao, W. Tian, Y. Wang, H. Zhang, *Inorg. Chem.* **2011**, *50*, 4825-4831; b) Z. Zhang, Z. Zhang, K. Ye, J. Zhang, H. Zhang, Y. Wang, *Dalton Trans.* **2015**, *44*, 14436-14443.

[33] M. Planells, N. Robertson, *Eur. J. Org. Chem.* **2012**, *2012*, 4947-4953.

[34] J. R. Lakowicz, *Principles of Fluorescence Spectroscopy*, Kluwer Academic/Plenum Publishers, New York, **1999**.

[35] A. J. Fry in *Laboratory Techniques in Electroanalytical Chemistry*, 2nd ed. (Eds.: P. T. Kissinger, W. R. Heineman), Marcel Dekker Ltd, New York, **1996**, p. 481.

Entry for the Table of Contents

Layout 1:

FULL PAPER

Boron-bridge to organic n-type semiconductors: Introduction of the boron-bridge into thienylthiazole and attachment of acceptor moieties allowed to obtain ambient-stable A-π-A molecules with low-lying LUMO levels. The materials were applied as active layers in OTFT devices. Enhanced electron mobility, measured for A-π-A systems bearing larger aromatic acceptor moieties, can be attributed to the effective 2D π-stacking in the solid state.

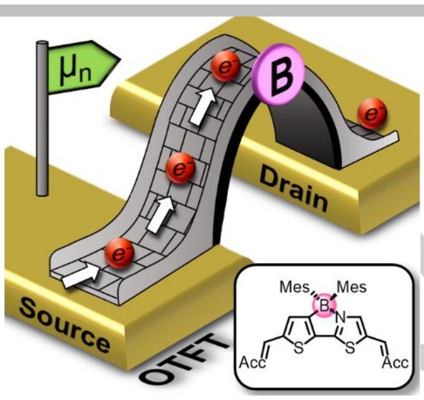

*Reinhard Hecht, Juliane Kade, David Schmidt, Agnieszka Nowak-Król**

Page No. – Page No.

n-Channel Organic Semiconductors Derived from Air-Stable Four-Coordinate Boron Complexes of Substituted Thienylthiazoles